Nonlocal kinetics of the electrons in a low-pressure afterglow plasma

Sergey Gorchakov* and Dirk Uhrlandt
INP Greifswald, Fr.-L.-Jahn-Strasse 19, Greifswald 17489, Germany

Michael J. Hebert and Uwe Kortshagen
Department of Mechanical Engineering, University of Minnesota-Twin Cities, 111 Church Street Southeast, Minneapolis, Minnesota 55455, USA

(Received 10 January 2006; published 11 May 2006)

Low-pressure pulsed plasmas are widely used in various technological applications. Understanding of the phenomena taking place in afterglow phase of the discharge makes possible the optimization of the operation conditions and improvement of the technical parameters. At low pressure the electron component of the plasma determines the main features of the discharge since its behavior dominates all other plasma properties. We study the electron kinetics in a low-pressure afterglow plasma of an inductively coupled discharge by means of a self-consistent model which uses the nonlocal kinetic approach. The main features of the model are given. Special attention is paid to determination of the steady state of the discharge from which the decay of the plasma begins. Emphasis is also put on the description of the collisional interaction between the electrons and gas. Results of theoretical investigations for argon at a pressure of 2–4 Pa are presented. Calculated temporal evolutions of the isotropic part of the electron velocity distribution function, electron density, mean electron energy, and wall potential are discussed in comparison with experimental data.

DOI: 10.1103/PhysRevE.73.056402 PACS number(s): 52.80.Pi, 52.25.Dg, 52.50.Qt

I. INTRODUCTION

In recent years nonisothermal plasmas have gained in importance due to their intensive use as light sources and for plasma processing. A high value of the electron mean energy, in comparison with the mean energies of neutrals and ions, gives the opportunity to initiate and control a variety of radiation and chemical processes. Pulsed operation has attracted special attention because pulse frequency, pulse form, and duty cycle can be used as additional control parameters to achieve specific plasma properties. The prediction of these properties by plasma modeling is still difficult, in particular in cases where the plasma-off duration is on the order of the decay time of relevant excited species in the plasma. One reason is that in these cases the time-averaged plasma properties are influenced to a large extent by complex particle interaction and redistribution processes not only in the active, but also in the afterglow phase. Therefore, plasma models have to be based on a detailed time-dependent treatment of the electron kinetics in the active as well as in the afterglow phase.

A large number of publications are devoted to a deeper understanding of the processes which govern the afterglow plasma, especially the relaxation processes of the electron energy. At sufficiently high gas pressure the collisions between electrons and neutral particles constitute the dominant energy loss process. Ionization of the long-living excited particles (i.e., metastable states) produces electrons with a high energy. However, both processes become negligible when the gas pressure is reduced down to few Pa. In contrast to this, the losses of the charge carriers due to ambipolar diffusion toward the walls become the most important processes for the energy balance of electrons. At low pressure, when the characteristic length of the energy relaxation due to the collision processes is larger than the plasma size, the electrons essentially conserve their total energy during the movement inside the plasma. Therefore, only the electrons with total energies exceeding the wall potential can reach the walls and recombine there. As a consequence, the electrons with high energy leave the plasma and the mean electron energy diminishes. This effect was first described in 1954 by Biondi [1] and denoted as "diffusive cooling." First investigations of this process have been performed by experiments [2,3] and by models [4,5] based on an analytical solution of the electron Boltzmann equation. Probe measurements in rare-gas plasmas [6–13] have shown different temporal behaviors of the electron density and mean electron energy in the afterglow phase. As investigations [6] indicate, at a pressure under 100 Pa the electron mean energy in the afterglow can decrease below the gas temperature due to the action of diffusive cooling. The investigations at higher pressures were focused on the influence of chemo-ionization processes [7–11,14] and their influence on the discharge reignition [15].

Different theoretical approaches have been used for investigations of afterglow phenomena. Simple models [7,8,11,13] include the solution of the electron energy balance coupled to approximations for ambipolar diffusion, energy losses in collisional processes, and energy gain due to chemo-ionization processes. The electron velocity distribution is obtained either from the solution of a drastically simplified kinetic equation [7,8] or by consideration of a Maxwellian distribution that is cut above the energy corresponding to the wall potential [11,13]. These models give an approximate description of the temporal evolutions of the energy losses of electrons due to ambipolar diffusion and of the electron tem-

*Electronic address: gorchakov@inp-greifswald.de

perature and of the wall potential during the afterglow in rare gas plasmas (Kr [7], Xe [8], He and Ne [11], Ar [13]), and allow a rough verification of measurements of the electron velocity distribution function [11,13]. However, such models require verification by a strict treatment of the time- and space-dependent electron kinetics and are not suitable for the description of both active and remote phases of pulsed plasmas.

Hydrodynamic models which avoid the kinetic description of the electron component are widely used for the description of pulsed plasmas [16–20]. Multidimensional models have been developed for the description of sheath dynamics in rf discharges [21] and inductively coupled discharges [22]; two- and three-dimensional (2D and 3D) models for the analysis of the plasma properties in inductively coupled plasma (ICP) reactors [23,24] are available. However, in these works less attention was paid to a detailed analysis of the electron component and to the afterglow behavior of the plasma.

In general, the determination of the electron velocity distribution function in afterglow plasmas requires the solution of the adequate time-dependent kinetic equation including the processes of electron-electron interaction (Coulomb collisions) as well as a treatment of the space-charge confinement, diffusive cooling, and the variety of collisional processes between electrons and various heavy particles. The solution of this complex problem is still unavailable. First attempts [25,26] were focused on the solution of the stationary kinetic equation with inclusion of Coulomb collisions for specified instants in the late afterglow. An Ar-N_2 discharge was described in Ref. [25], neglecting the process of ambipolar diffusion. In Ref. [26] the so-called "nonlocal approach" [27] for the kinetic equation was used, taking into account the ambipolar diffusion. Diffusive cooling was described by solving an inhomogeneous Boltzmann equation in the high-energy range.

In low-pressure plasmas the kinetics of the electrons shows a pronounced nonlocal character [28–30]. Therefore, the kinetic equation must include the space-dependent terms. In the first approximation this could be done by use of the nonlocal approach [27].

The first strict treatment of the diffusive cooling process for low-pressure afterglow plasma has been performed in the work of Arslanbekov *et al.* [31]. For a low-pressure model plasma the time- and space-dependent kinetic equation was solved applying the nonlocal approach. The model took into account the outflux of the electrons with energies higher than the wall potential and, hence, the diffusive cooling process. Special attention was paid to the electron-electron interaction, which is the only process acting against the diffusive cooling at pressures of several Pa. The temporal evolution of the wall potential was obtained using simplified balances for the charge carriers and assuming a fixed potential profile. The method presented in Ref. [31] gave a qualitative picture of the interaction between electron-electron collisions and diffusive cooling in low-pressure decaying plasmas. However, the model had limitations for the investigations of real plasmas, since it started with a Maxwellian distribution and neglected the collisional interaction between the electrons and gas. Such an interaction, especially the production of high-energy electrons due to stepwise and chemo-ionization, is of great importance when the pressure is increased up to 100 Pa. Therefore, an appropriate extension of this model is necessary to treat a real gas discharge situation.

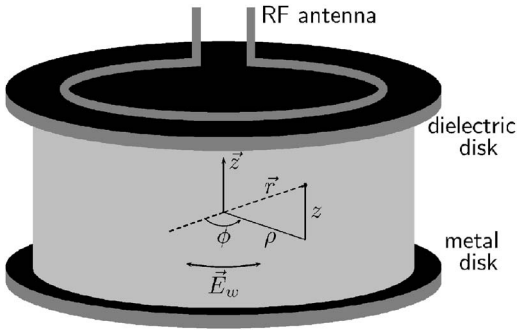

FIG. 1. Discharge geometry considered in the model.

In the framework of the present paper the early afterglow—i.e., the range of few microseconds after switching off the power input—in an argon plasma at pressures of few Pa is studied. As an example, an inductively coupled discharge in a cylindrical vessel of few cm height is considered. The study focuses on the electron kinetic behavior which dominates all other plasma properties under these conditions. Special attention is paid to inclusion of the collisional interaction between electrons and the gas and of the chemo-ionization processes. In contrast to other works [13,31], where a Maxwellian distribution was chosen as a starting situation, the description of the afterglow starts from a steady-state solution of the whole equation system for the active discharge phase considering a spatially homogeneous azimuthal rf field. For the verification of the model a detailed comparison with Langmuir probe measurements is performed.

The applied methods for the self-consistent plasma description are presented in Sec. II. First results are discussed in Sec. III.

II. BASIC FEATURES OF THE MODEL

Figure 1 presents the discharge geometry considered in the model, which emulates the dimensions of the experimental setup used for the probe measurements [13]. A diffusive plasma is confined between relatively large dielectric or floating metal disks with a diameter of 28 cm in a distance d of 4–10 cm. The plasma is produced by an rf field $\vec{E}_w$ which acts in the azimuthal direction at a field frequency of 13.56 MHz. In contrast to the real experiments, the discharge is assumed to be axially symmetric and spatially homogeneous in radial (ρ) and azimuthal (ϕ) directions. The spatial dependence is reduced to the treatment of the plasma confinement by the time-dependent space-charge potential $V(z,t)$ in the axial (z) direction. This is a good approximation for the situations of the experiments reported here, since the large aspect ratio (radius:height) considered here causes the spatial transport in axial direction to dominate over that in radial direction.

The model for the investigations of the temporal decay in the afterglow plasma consists of the time- and space-

dependent electron kinetic equation and of a simplified model for determination of the axial space-charge potential.

The collisional model for argon distinguishes five states within argon energy levels: the ground-state Ar($1p_0$), three lumped excited states—i.e., metastable state Ar(m), resonant state Ar(r), and excited state Ar($*$), which includes ten $2p$ levels of argon, and the Ar^+ ion in the ground state. Since the early afterglow is considered, the densities are assumed to be time independent. The density of the ground-state atoms is also assumed to be space independent, while the fixed axial profiles are used for the excited-state densities. The axis values of the densities of the excited states have been estimated from experimental data of Ref. [32] where the discharge at similar conditions was studied.

Details of the basic equations, the atomic data, and the solution method used are given in the following subsections.

A. Time-dependent electron Boltzmann equation

The electron kinetics is determined by the time- and space-dependent Boltzmann equation

$$\frac{\partial F}{\partial t} + \vec{v}\cdot\vec{\nabla}_{\vec{r}}F - \frac{e_0}{m_e}\vec{E}\cdot\vec{\nabla}_{\vec{v}}F = C^{el}(F) + C^{in}(F) + C^{ee}(F) + C^{ch} \tag{1}$$

for the velocity distribution function $F(\vec{r},\vec{v},t)$ for the electrons with charge $-e_0$ and mass m_e. The right-hand side of Eq. (1) includes collision integrals for various elastic C^{el}, inelastic C^{in}, and electron-electron C^{ee} collisions and chemoionization C^{ch}. Taking into account the radial and azimuthal homogeneity of the plasma two components of the electric field have to be considered: $\vec{E}=E_w(t)\cdot\vec{e}_\phi+E_z(z,t)\cdot\vec{e}_z$, the heating azimuthal rf field $E_w(t)$, and confining axial space-charge field $E_z(z,t)$.

According to the specific symmetry of the plasma the velocity distribution can be presented by the two-term expansion

$$F\left(z,u,\frac{\vec{v}}{v},t\right) = \frac{1}{2\pi}\left(\frac{m_e}{2}\right)^{3/2}\left[\hat{f}_0(z,u,t) + \hat{f}_\phi(z,u,t)\frac{v_\phi}{v} + \hat{f}_z(z,u,t)\frac{v_z}{v}\right] \tag{2}$$

in spherical harmonics, where $\hat{f}_0$, $\hat{f}_\phi$, and $\hat{f}_z$ are the isotropic distribution and the azimuthal and axial components of the vectorial anisotropic part of the distribution, $u=m_e v^2/2$ is the kinetic energy, and z denotes the axial coordinate. The discussion of limitations of the two-term approximation of electron kinetic theory presented recently in Ref. [33] shows that this theory works well for the parameter range studied. After the substitution of expansion (2), the kinetic equation (1) is transformed into a system of equations for the expansion coefficients $\hat{f}_0$, $\hat{f}_\phi$, and $\hat{f}_z$.

Since the plasma confinement in one spatial direction is considered, it is convenient to transform the equation system to a total energy ε which is the sum of kinetic energy u and the potential energy $w(z,t)=-e_0V(z,t)$ in the axial space-charge field $E(z,t)=-\mathrm{d}V(z,t)/\mathrm{d}z$ according to

$$\tilde{f}_x(z,\varepsilon,t) = \hat{f}_x(z,u(z,\varepsilon),t), \quad x=0,z,\phi. \tag{3}$$

When the plasma of a low-pressure discharge is considered, the collisional interaction of the electron component with the gas atoms is weak. The electrons move in the plasma with nearly constant total energy ε. Under these conditions the so-called nonlocal approach can be applied for the description of the electron kinetic behavior [27,34]. In the frame of the nonlocal approach the axial dependence of the isotropic distribution as a function of the total energy is neglected; i.e., the assumption

$$\tilde{f}_0(z,\varepsilon,t) = f_0(\varepsilon,t) + \tilde{f}_0^{(1)}(z,\varepsilon,t) \approx f_0(\varepsilon,t) \tag{4}$$

is adopted. This corresponds with the assumption that $\tilde{f}_z$ goes to zero. Finally, after elimination of the f_ϕ component, the equation for distribution function $f_0(\varepsilon)$ is obtained by integrating at fixed total energy ε the kinetic equation over the relevant area of the plasma cross section in the (z,ε) space according to

$$\frac{1}{z_e}\int_0^{z(\varepsilon)} \{\text{kinetic equation}\}dz, \tag{5}$$

with

$$z(\varepsilon) = \begin{cases} z \quad \text{with } \varepsilon = w(z) & \text{for } 0 \leqslant \varepsilon < w(z_e), \\ z_e & \text{for } w(z_e) \leqslant \varepsilon, \end{cases} \tag{6}$$

where z_e denotes the axial size of the plasma measured from the center—i.e., the half of the distance between the metal disks ($d=2z_e$). After all transformations the simplified kinetic equation takes the form

$$\sqrt{\frac{m_e}{2}}\left(\hat{B}\frac{\partial f_0}{\partial t} + \hat{C}\frac{\partial f_0}{\partial \varepsilon}\right) + L_w f_0 - \frac{\partial}{\partial\varepsilon}\left(\hat{D}\frac{\partial f_0}{\partial\varepsilon}\right) - \frac{\partial}{\partial\varepsilon}(\hat{G}f_0) + \hat{H}f_0 - Y\frac{\partial}{\partial\varepsilon}\left[\frac{2}{3}\left(\int_0^\varepsilon \hat{A}f_0 d\varepsilon' + \hat{A}\int_\varepsilon^\infty f_0 d\varepsilon'\right)\frac{\partial f_0}{\partial\varepsilon} + f_0\int_0^\varepsilon \hat{B}f_0 d\varepsilon'\right] = \hat{S}_0 + \hat{S}_c, \tag{7}$$

with the coefficients

$$\hat{A}(\varepsilon) = \frac{1}{z_e}\int_0^{z(\varepsilon)} u^{3/2}dz, \tag{8a}$$

$$\hat{B}(\varepsilon) = \frac{1}{z_e}\int_0^{z(\varepsilon)} u^{1/2}dz, \tag{8b}$$

$$\hat{C}(\varepsilon) = \frac{1}{z_e}\int_0^{z(\varepsilon)} u^{1/2}\frac{\partial w}{\partial t}dz, \tag{8c}$$

$$\hat{G}(\varepsilon) = \frac{1}{z_e}\int_0^{z(\varepsilon)} u^2\left(\sum_k \frac{2m_e}{M_k}N_k(z)Q_k^m(u)\right)dz, \tag{8d}$$

$$\hat{D}(\varepsilon) = \frac{(e_0 E_w)^2}{3 z_e} \int_0^{z(\varepsilon)} \frac{u^2 \sigma_t}{u \sigma_t^2 + (2\pi \nu_{rf})^2} dz + k T_g \hat{G}, \quad (8e)$$

$$\hat{H}(\varepsilon) = \frac{1}{z_e} \int_0^{z(\varepsilon)} u \sigma^{\mathrm{in}} dz, \quad (8f)$$

$$L_w(\varepsilon) = \begin{cases} 0 & \text{for } \varepsilon \leqslant w(z_e), \\ \dfrac{1-\zeta}{1+\zeta} \dfrac{u}{2 z_e} & \text{for } \varepsilon > w(z_e), \end{cases} \quad (8g)$$

$$\hat{S}_0(\varepsilon, f_0) = \sum_i \left(\frac{1}{z_e} \int_0^{z(\varepsilon)} (u + U_i^{\mathrm{in}}) N_i(z) Q_i^{\mathrm{in}}(u + U_i^{\mathrm{in}}) dz \right) f_0(\varepsilon + U_i^{\mathrm{in}}) + 4 \sum_j \frac{1}{z_e} \int_0^{z(\varepsilon)} (2u + U_j^{\mathrm{io}}) N_j(z) Q_j^{\mathrm{io}}(2u + U_j^{\mathrm{io}}) f_0(\varepsilon + u + U_j^{\mathrm{io}}) dz, \quad (8h)$$

$$\hat{S}_c(\varepsilon) = \sqrt{\frac{m_e}{2}} \sum_l \sum_k \frac{1}{z_e} \int_0^{z(\varepsilon)} z_{l,k}^{\mathrm{ch}} N_l(z) N_k(z) u^{1/2} P_{l,k}(u) dz, \quad (8i)$$

where

$$\sigma^{\mathrm{in}}(z,u) = \sum_i N_i(z) Q_i^{\mathrm{in}}(u) + \sum_j N_j(z) Q_j^{\mathrm{io}}(u), \quad (9)$$

$$\sigma_t(z,u) = \sigma^{\mathrm{in}}(z,u) + \sum_k N_k(z) Q_k^m(u), \quad (10)$$

$$u(z,\varepsilon) = \varepsilon - w(z,t), \quad (11)$$

Q_m^k denotes the cross section for momentum transfer in elastic collisions, Q_i^{in} and Q_j^{io} are the total cross sections of the inelastic and ionizing collision processes, and U_i^{in} and U_j^{io} the corresponding energy losses. The model considers the collisional interaction of the electrons with atoms of densities $N_l(z)$ and mass M_l presented in the collisional integrals. The quantity Y in the Fokker-Planck term is given by the expression

$$Y = \frac{e_0^4}{8\pi\epsilon_0^2} \ln \Lambda, \quad \Lambda = \frac{8\pi}{e_0^3} \sqrt{\frac{2\epsilon_0^3 u_e^3(0)}{3 n_e(0)}}, \quad (12)$$

where $n_e(0)$ and $u_e(0)$ denote the density and mean energy of electrons at the discharge center and ϵ_0 is the permittivity of the free space. The in-scattering probability of the electrons, produced by chemo-ionization process $P_{l,k}(u)$, is given by

$$P_{l,k}(u) = \frac{3}{4} \frac{1}{u_w^{l,k} u^{1/2}} \left[1 - \left(\frac{u - u_c^{l,k}}{u_w^{l,k}} \right)^2 \right], \quad (13)$$

where $u_c^{l,k}$ and $u_w^{l,k}$ characterize the center and width of the in-scattering profile in energy space.

The wall losses of electrons are treated by a loss term L_w which vanishes for total energies smaller than the potential energy corresponding to the space-charge potential at the wall. The expression for the loss term is derived from the consideration of the global electron particle balance which is obtained from an integration of the Boltzmann equation. The electron loss in the z direction is determined by the anisotropy component f_z of the electron distribution function. After averaging over the z direction according to Eq. (5) this balance becomes

$$\frac{\partial \langle n_e \rangle}{\partial t} + \frac{j_z(z_e)}{z_e} = P^{\mathrm{io}}, \quad (14)$$

with

$$j_z(z_e) = \frac{1}{3} \sqrt{\frac{2}{m_e}} \int_{w(z_e)}^{\infty} f_z(\varepsilon) u d\varepsilon, \quad (15)$$

$$P^{\mathrm{io}} = \frac{1}{z_e} \sqrt{\frac{2}{m_e}} \int_0^{\infty} \left(\sum_j \int_0^{z(\varepsilon)} u N_j Q_j^{\mathrm{io}} dz \right) f_0(n,t) d\varepsilon + \sqrt{\frac{2}{m_e}} \int_0^{\varepsilon} \hat{S}_c(\varepsilon, t) d\varepsilon. \quad (16)$$

Here $j_z(z_e)$ denotes the current density at the wall and P^{io} is the ionization rate. A boundary condition corresponding to Eq. (21b) in Ref. [35] is used to relate f_z to f_0 in front of the wall. The assumption of a thin collisionless sheath is avoided here by resolving potential distribution in the sheath according to an appropriate model potential (see Sec. II C). Considering electron reflection at the wall with a coefficient ζ results in the relation

$$f_z(\varepsilon)|_{z=z_e} = \frac{3}{2} \frac{1-\zeta}{1+\zeta} f_0(\varepsilon \geqslant w(z_e)). \quad (17)$$

Correspondingly, L_w gets the form given in Eq. (8g). In present calculations we assume ζ to equal 0.5.

The term with the coefficient $\hat{D}$ [see Eq. (8f)] treats the power input in the kinetic equation due to an electric field [first term Eq. (8f)] and collisions with gas atoms [second term in Eq. (8f)]. The field heating is considered in the active phase of the discharge and vanishes in the afterglow phase. For the description of an inductive heating by an azimuthal rf field, for simplicity, the high-frequency approach [36–38] considering a spatially homogeneous field with frequency ν_{rf} and amplitude E_w has been applied. This approach assumes that the isotropic component of the electron velocity distribution function is almost constant in time during the rf period and the corresponding anisotropic component (here the azimuthal one) changes with the rf field with a certain phase shift. Such an approach is applicable for the rf field frequency of 13.56 MHz at few Pa argon pressure.

B. Electron and heavy-particle collision data

The set of electron–heavy-particle collisions has been selected from the literature. The data for excitation processes among the argon states have been compiled from the data set of Zeman *et al.* [39,40], obtained with the Breit-Pauli *R*-matrix method. This cross-section set coinsides well with recent experimental data for individual excitation in argon of Boffard *et al.* [41] and reproduces the experimental total ex-

citation cross section of Schaper and Scheibner [42]. The cross sections for deexcitation have been obtained according to the principle of detailed balancing. The cross section of direct ionization of argon atoms is taken from Ref. [43]. Those for stepwise ionization have been calculated according to the Deutsch-Märk formalism [44] which could be easily extended for determination of cross sections for individual argon states due to its simplicity. The data for elastic collision process for argon are taken from Ref. [45].

In the pressure range of 1–100 Pa chemo-ionization could become one of the most important processes of electron production. Moreover, chemo-ionization is a source of the electrons with a high energy and, therefore, acts against the diffusive cooling of the electron gas. The contribution of this process to the electron particle and energy balances is proportional to the densities of colliding particles. Therefore, the ionizing collisions between the most populated excited argon levels Ar(m) and Ar(r) were taken into account. The rate coefficients $z_{l,k}^{\mathrm{ch}}$ $(l,k=1,2)$ are estimated according to Ref. [46]. The energy distribution of the in-scattered electrons is assumed to have a Gaussian shape [see Eq. (13)] with a width $u_w^{l,k}$ of 1.5 eV. Following the experimental results [10,47], the center of a Gauss profile is chosen to be equal to the energy $u_c^{l,k}=U_1^{\mathrm{ex}}+U_2^{\mathrm{ex}}-U^{\mathrm{io}}$, where U_i^{ex} and U^{io} denote the excitation and ionization thresholds of colliding particles.

C. Description of the space-charge potential

The model includes a simplified description of the space-charge potential. The polynomial representation

$$V(z,t)=V_0(t)\left[0.7\left(\frac{z}{z_e}\right)^2+0.3\left(\frac{z}{z_e}\right)^{12}\right] \tag{18}$$

is used for simplicity with the fixed coefficients 0.7 and 0.3. Such a model potential corresponds sufficiently well to the results of self-consistent calculations and measurements in space-charge confined plasmas at low pressure (see, e.g., Refs. [48–52]). Notice that the collapse of the wall potential in a decaying plasma can lead to changes in the radial profile of the potential. However, such changes are expected to be significant in the late afterglow only. On the other hand, as long as the nonlocal kinetic approach is assumed to be valid, the shape of the potential is of minor importance, since an averaging procedure over the space is applied.

As in Ref. [13], the ion flux is determined by considering an appropriate diffusion length Λ and ambipolar diffusion coefficient $D_{\mathrm{amb}}=D_{\mathrm{i}}+D_{\mathrm{e}}b_{\mathrm{i}}/b_{\mathrm{e}}$ and assuming a cosine form for the axial density profile of the argon ions $n_{\mathrm{i}}(z)=n_{\mathrm{i}}(0)\cos(z/\Lambda)$. The diffusion coefficient for argon ions is determined using the Einstein relation and temperature-dependent mobility of argon ions b_{i}. The electron transport coefficients are determined for each time step from the isotropic distribution according to

$$b_{\mathrm{e}}(z,t)=\frac{1}{3}\frac{1}{n_{\mathrm{e}}(z)}\sqrt{\frac{2}{m_{\mathrm{e}}}}\int_{\varepsilon=w(z)}^{\infty}\frac{1}{\sigma_t}\frac{\partial f_0(\varepsilon,t)}{\partial\varepsilon}ud\varepsilon, \tag{19}$$

$$D_{\mathrm{e}}(z,t)=\frac{1}{3}\frac{1}{n_{\mathrm{e}}(z)}\sqrt{\frac{2}{m_{\mathrm{e}}}}\int_{\varepsilon=w(z)}^{\infty}\frac{1}{\sigma_t}f_0(\varepsilon,t)ud\varepsilon. \tag{20}$$

For the determination of the ambipolar diffusion coefficient the values of the electron transport coefficients at the wall have been used. Neglecting the distortion of quasineutrality the drop of the ion density can be written as

$$\frac{dn_{\mathrm{i}}}{dt}=P^{\mathrm{io}}-n_{\mathrm{e}}(0)\frac{D_{\mathrm{amb}}}{\Lambda^2}. \tag{21}$$

The ionization rate P^{io} is given by Eq. (16). Following Refs. [13,53] the diffusion length is determined from an assumption that the density profile produces a diffusion flux $\Gamma_i=-D_{\mathrm{amb}}\nabla n|_s$ at the sheath boundary that matches the Bohm flux $n_s\sqrt{2u_e/3M_{\mathrm{i}}}$. The subscript s indicates the density and gradient at the boundary of the sheath that is assumed to be of negligible thickness. This consideration leads to following transcendental equation for Λ:

$$\tan\left(\frac{z_e}{\Lambda}\right)=\sqrt{\frac{2u_{\mathrm{e}}}{3M_{\mathrm{i}}}}\frac{\Lambda}{D_{\mathrm{amb}}}. \tag{22}$$

The value of the wall potential V_0 is finally determined for every time step by repeating the electron kinetic and the ion flux description for varying potential until electron and ion particle fluxes to the wall are equal—i.e., neglecting possible small deviations from the ambipolarity in the time evolution:

$$n_{\mathrm{e}}(0)\frac{D_{\mathrm{amb}}}{\Lambda^2}=\frac{j_z(z_e)}{z_e}=\sqrt{\frac{2}{m_{\mathrm{e}}}}\int_{w(z_e)}^{\infty}L_w f_0 d\varepsilon. \tag{23}$$

D. Solution approach

The description of the decaying plasma is separated into two tasks: (i) determination of the steady-state discharge parameters and (ii) the afterglow from this state. Figure 2 shows the scheme of the solution approach for the determination of the steady-state plasma parameters. The calculations start with given experimental electron density and first estimates for the rf field amplitude and the wall potential. Two enclosed iterative cycles which are necessary to take into account the backscattering term $S_0(\varepsilon,f_0)$ and the terms describing electron-electron interaction analogous to [54] provide the solution for the electron Boltzmann equation. A specific method introducing a control parameter u_{e} into the Fokker-Planck term as described in [54] is applied to provide the fulfilment of the electron power balance. With the resulting distribution function the transport coefficients according to Eqs. (19) and (20) are calculated and used to determine the ambipolar diffusion coefficient D_{amb}. The new amplitude of the rf field is chosen in such a way that the the mean ionization rate P^{io} compensates for the ambipolar loss of the electrons. After checking the compensation of the ion flux to the wall by the electron flux calculated according to Eq. (23), the new value of the wall potential that leads to this compensation is estimated. The solution procedure iterates until a steady state of all parameters and the fulfillment of all mentioned balances is reached.

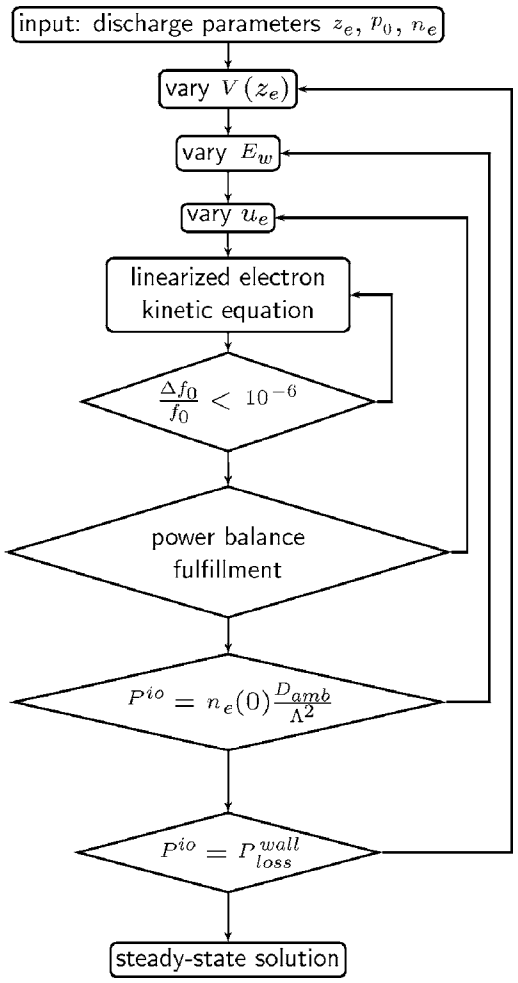

FIG. 2. The algorithm for determination of the steady-state plasma parameters.

A similar solution approach is used to describe the decaying plasma. The afterglow starts with switching off the rf field within a certain time period. The electron density is now determined from the temporal evolution of the isotropic distribution. For each time step the rf field amplitude is given. Starting with an estimated value of the space-charge potential the linearized electron kinetic equation is solved. The stabilizing effect of the time derivative of the disctribution function leads to a sufficient fulfillment of the electron power balance without using a specific control method for the treatment of the Fokker-Planck term (cycle over u_e in Fig. 2). With the resulting distribution function the transport coefficients and the particle wall losses of the electrons are calculated. These data are used then to determine a new value of the wall potential which should lead to compensation of the electron and ion fluxes at the wall. The time step solution is finished when such compensation is reached. The check of the electron particle and power balances as well as the relative changes of the distribution function over one time step are used after a couple of time steps for estimation of a new time step duration.

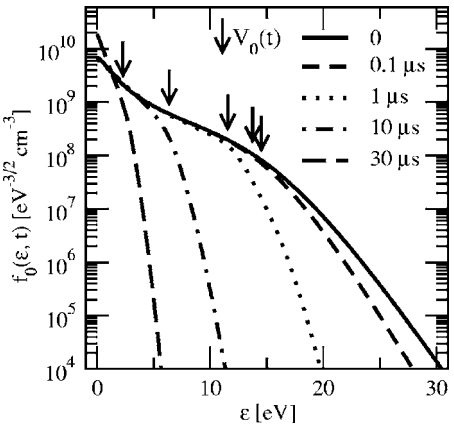

FIG. 3. Temporal evolution of the isotropic distribution $f_0(\varepsilon,t)$ in the discharge center (z=0) during the early afterglow for set A.

III. RESULTS AND DISCUSSION

In order to compare the results of calculations with the experiments two parameter sets which are characterized by different gas pressures and geometries have been used. Set A has a gas pressure of 2 Pa and the distance between the disks d of 10 cm (z_e=5 cm). The pressure of 4 Pa and the separation of 4 cm (z_e=2 cm) are further denoted as parameter set B. Experimental results for set A were published in Ref. [13]; corresponding results for set B have been obtained in recent measurements in the same experimental setup as used in [13]. For details of the experimental setup and the measurement procedure, the reader is referred to Ref. [13].

Figure 3 shows the calculated temporal evolution of the isotropic distribution during the first 30 μs in the afterglow for set A. The afterglow studies start at t=0 μs from the steady state. The decay is forced by switching off the electric field from the value of about 0.74 V/cm (steady-state solution for given $n_e=2.5\times10^{10}$ cm^{-3}) to zero. The decay time of the rf power was measured from the experimental setup used. The steady-state distribution shows a pronounced non-Maxwellian structure. The peak in the energy region between 0 and 5 eV results from the Ramsauer effect in argon enhanced by a specific heating of the electrons by a rf field where the electrons with a low energy gain less energy from the field. The depletion of the isotropic distribution at the energies higher than 15 eV in steady state results not only from energy loss in inelastic electron-atom collisions with the Ar ground state, but also from the action of diffusive cooling. The energy at which the change of the slope of the distribution function occurs corresponds to the wall potential (shown in the figure by arrows), which is equal to 15.1 V at this instant (see Fig. 4). The decay of the wall potential with time causes a shift of this specific energy towards lower energies. For example, at t=10 μs the potential is about 6 V and the change of the distribution slope also takes place around 6 eV. Notice that at this instant the electrons do not reach sufficient energy for inelastic collisions with Ar ground state which dominate at low pressure (the first threshold is around 11.55 eV), and only the electron wall loss is responsible for the diminishing population of electrons at higher energies. The electrons which have an energy higher than

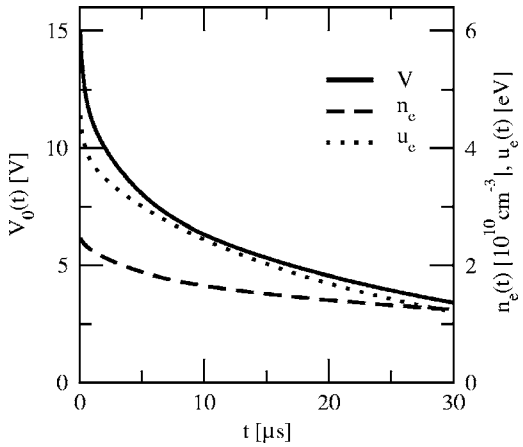

FIG. 4. Decay of the wall potential $V_0(t)$ and the axis values of the electron density $n_e(t)$ and mean electron density $u_e(t)$ for set A.

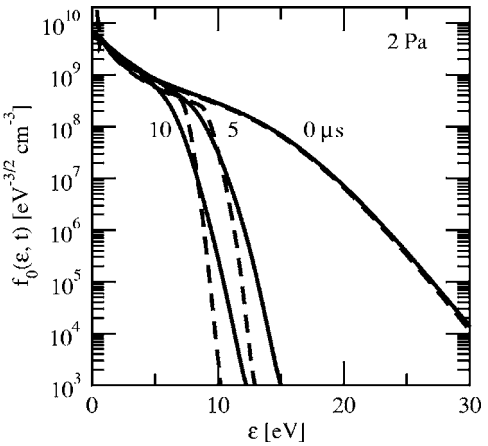

FIG. 5. Comparison between the calculated evolutions of the isotropic distribution $f_0(\varepsilon,t)$ with (solid lines) and without (dashed lines) inclusion of electron-electron collisions for set A.

eV_0 escape from the plasma and recombine at the wall. In this way the high-energy part of the isotropic distribution undergoes strong depletion in contrast to the energy range below eV_0. The population of this energy domain remains nearly unchanged until $t=12$ μs. Further temporal evolution of the distribution function is accompanied by a remarkable increase of the population in the low-energy region. Therefore, the electron density drops by only the factor of 2.5 during the first 30 μs in the afterglow (see Fig. 4), starting from the steady-state value of about 2.5×10^{10} cm^{-3}. The depletion of the high-energy part of the distribution function causes a decrease of the mean energy from about 5 eV in the steady state to about 1.1 eV at $t=30$ μs. Thus, the mean electron energy in the afterglow plasma diminishes faster than the electron density.

The turnoff of the rf electric field causes a redistribution of the power input and gain processes. Three kinds of processes are responsible for the production of high-energy electrons in the afterglow. (i) Superelastic collisions with excited atoms lead to the appearance of a group of high-energy electrons. This group is expected to influence the population of the electron distribution in argon around 11.55 eV. (ii) Chemo-ionization processes cause an enrichment of the distribution function nearby the characteristic energy equal to the difference between the sum of excitation thresholds of colliding particles and the ionization threshold (in argon around 7.3 eV). Due to the low density of excited argon atoms in the considered pressure range, these two kinds of processes have an insignificant influence on the plasma characteristics only. (iii) The electron-electron interaction forces a redistribution of the energy inside the electron ensemble, leading to a growth of the distribution function at high energies. The impact of the e-e interaction on the temporal evolution of the isotropic distribution during the first 10 μs in the afterglow is illustrated in Fig. 5. The calculated electron distribution functions almost coincide at steady-state conditions. However, in the afterglow phase a steeper drop of the high-energy part of $f_0(\varepsilon,t)$ occurs when Coulomb collisions are neglected. The wall potential in the case with an electron-electron interaction diminishes faster due to a higher value of the ionization rate [Eq. (18)] and, hence, higher values of the fluxes of the charge particles which should be compensated by the potential drop.

A similar behavior of the plasma properties has been obtained from the calculations for a discharge at 4 Pa and a disk distance of 4 cm (set B).

Figure 6 demonstrates a comparison between the calculated temporal evolutions of the isotropic distribution and results of Langmuir probe measurements for both geom-

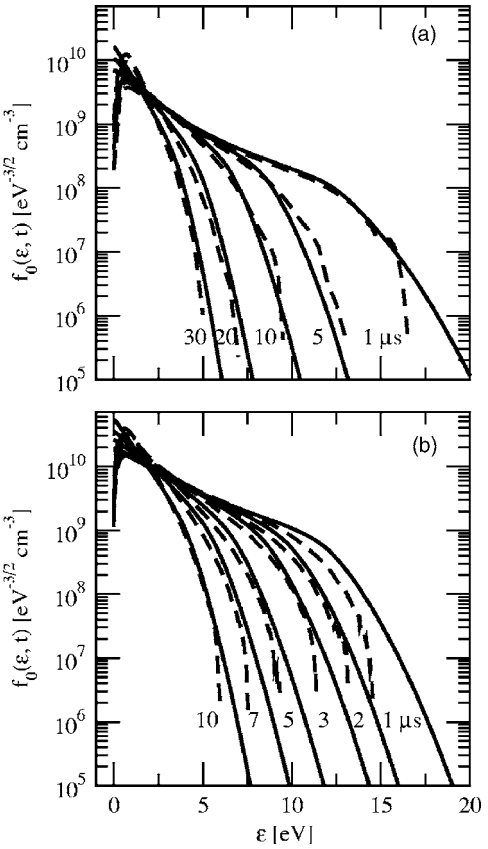

FIG. 6. Comparison between the calculated (solid lines) and measured (dashed lines) evolutions of the isotropic distribution $f_0(\varepsilon,t)$ for set A (a) and set B (b).

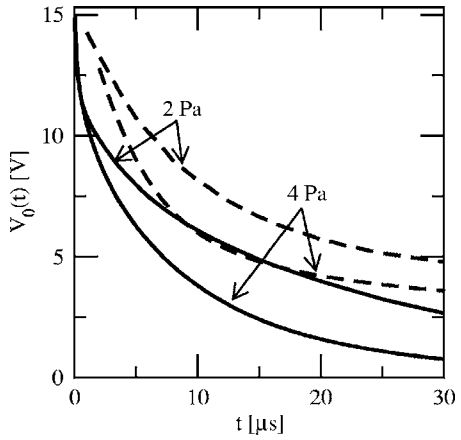

FIG. 7. Temporal behavior of the wall potential V_0 at different pressures and electrode distances. Solid lines: calculations. Dashed lines: measurements.

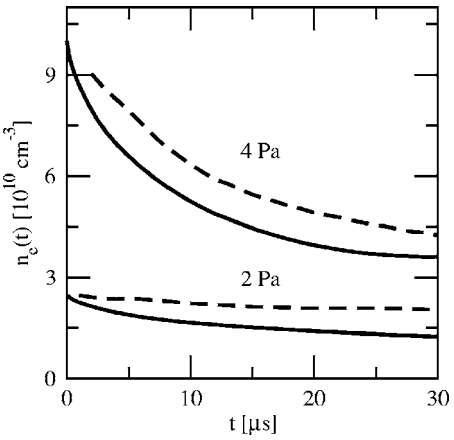

FIG. 8. Comparison between the calculated (solid lines) and measured (dashed lines) evolutions of the electron density in dependence on the gas pressure and discharge geometry.

etries. Good agreement between the respective data is obtained for the considered parameter range. The discrepancies at energies below 2 eV can originate from simplifications made in the model as well as from difficulties of determination of the space-charge potential in the probe measurements. In addition, the assumption of the radial homogeneity of the plasma is not fulfilled in the experiments. Especially in the case with smaller axial distance (set B) the discharge shows a more pronounced radial structure [32,55,56].

The measured and calculated temporal evolutions of the wall potential at the two discharge conditions are compared in Fig. 7. Because of the weak collisional interaction for the conditions under consideration, a slower decrease of the wall potential at higher pressure should be expected [13]. However, the smaller height of the plasma leads to enhanced ambipolar losses; therefore, the potential decay occurs faster for set B despite the higher pressure. The results of calculations are in good qualitative agreement with experimental data. The differences in the quantitative description arise probably from the simplified model for the determination of the wall potential.

The evolutions of the calculated and measured electron densities and mean electron energies are shown in Figs. 8 and 9, respectively. Generally, reasonable agreement for the tendencies as well as for the absolute values has been obtained. Calculated absolute values of the electron densities are lower than those from the probe measurements. A stronger decrease of the electron density in the case of set B during the first 15 μs is caused by the higher loss frequency due to the ambipolar diffusion. After this instant the decay of the wall potential occurs slower. This leads to a stabilization of the number of the electrons which are able to reach the wall and recombine there. Therefore, the electron density decay rate also decreases in particular at higher pressure.

The calculated decay of the mean electron energy shows similar tendencies as the density. However, the mean electron energy in the afterglow plasma diminishes much faster than the electron density. As was already mentioned above in case A the mean electron energy drops by about factor of 5. In the case of set B the value of the mean energy decreases even by factor of 30. The steady-state electron density exceeds the density at 30 μs by a factor of 2 in the case of set A and by factor 3 in the case of set B.

IV. SUMMARY

A self-consistent model based on the nonlocal kinetic approach of the electron component has been applied to study the afterglow plasma in a low-pressure argon discharge in the pressure range 2–4 Pa. The model includes a description of the steady-state plasma parameters and takes into account the complex collisional interaction in plasma. The calculated temporal evolutions of the isotropic distribution, density, and mean electron energy of electrons as well as of the wall potential have been compared with the results of Langmuir probe measurements. Good agreement between these data is found. The model predicts that the mean electron energy in the afterglow plasma decreases faster than the electron density.

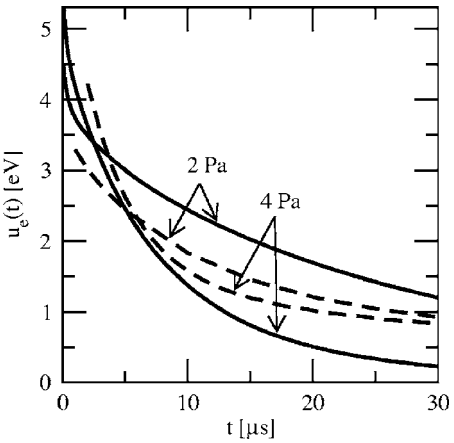

FIG. 9. Comparison between the calculated (solid lines) and measured (dashed lines) evolutions of the mean electron energy at different gas pressures and discharge geometries.

Extensions of the model concerning a more detailed treatment of the space-charge confinement and of the excited plasma species are planned for future work. This should expand the applicable range of the model towards higher pressures.

ACKNOWLEDGMENTS

The work is supported by the Deutsche Forschungsgemeinschaft Project No. Uh 106/2-1. M.H. and U.K. acknowledge support by the U.S. Department of Energy under Grant No. ER54554 for the experimental part of this study.

[1] M. A. Biondi, Phys. Rev. **93**, 1136 (1954).
[2] M. J. Mulcahy and J. J. Lennon, Proc. Phys. Soc. London **80**, 626 (1962).
[3] T. Rhymes and R. Crompton, Aust. J. Phys. **28**, 675 (1975).
[4] J. H. Parker, Phys. Rev. **139**, A1792 (1965).
[5] R. Robson, Phys. Rev. A **13**, 1536 (1976).
[6] M. Suguwara, T. Okada, and Y. Kobayashi, J. Phys. D **19**, 1213 (1986).
[7] N. Kolokolov, A. Kudryavtsev, and O. Toronov, Sov. Phys. Tech. Phys. **30**, 1128 (1985).
[8] V. Demidov, N. Kolokolov, and O. Toronov, Sov. J. Plasma Phys. **12**, 402 (1988).
[9] T. Bräuer, S. Gortchakov, D. Loffhagen, S. Pfau, and R. Winkler, J. Phys. D **30**, 3223 (1997).
[10] L. J. Overzet and J. Kleber, Plasma Sources Sci. Technol. **7**, 512 (1998).
[11] N. A. Gorbunov, N. B. Kolokolov, and F. E. Latyshev, Sov. Phys. Tech. Phys. **46**, 391 (2001).
[12] H. Bäcker, J. W. Bradley, P. J. Kelly, and R. D. Arnell, J. Phys. D **34**, 2709 (2001).
[13] A. Maresca, K. Orlov, and U. Kortshagen, Phys. Rev. E **65**, 056405 (2002).
[14] T. Okada and M. Sugawara, J. Phys. D **35**, 2105 (2002).
[15] Z. L. Petrovic, V. L. Markovic, M. M. Pejovic, and S. R. Gogic, J. Phys. D **34**, 1756 (2001).
[16] T. C. Wei, L. R. Collins, and J. Philips, J. Phys. D **28**, 295 (1995).
[17] S. Ashida, C. Lee, and M. Lieberman, J. Vac. Sci. Technol. A **13**, 2498 (1995).
[18] M. Lieberman and S. Ashida, Plasma Sources Sci. Technol. **5**, 145 (1996).
[19] D. Lymberopoulos, V. I. Kolobov, and D. J. Economou, J. Vac. Sci. Technol. A **16**, 564 (1998).
[20] V. Midha and D. J. Economou, Plasma Sources Sci. Technol. **9**, 256 (2000).
[21] th. Panagopoulos and D. J. Economou, J. Appl. Phys. **85**, 3435 (1999).
[22] G. Wenig, P. Scheubert, and P. Awakowicz, Surf. Coat. Technol. **174–175**, 482 (2003).
[23] S. K. Nam and D. J. Economou, J. Appl. Phys. **95**, 2272 (2004).
[24] Th. Panagopoulos, D. Kim, V. Midha, and D. J. Economou, J. Appl. Phys. **91**, 2687 (2002).
[25] N. A. Dyatko, Y. Z. Ionikh, N. B. Kolokolov, A. V. Meshanov, and A. P. Napartovich, J. Phys. D **33**, 2010 (2000).
[26] R. R. Arslanbekov and A. A. Kudryavtsev, Phys. Rev. E **58**, 7785 (1998).
[27] L. D. Tsendin, Sov. Phys. JETP **39**, 805 (1974).
[28] V. I. Kolobov and V. A. Godyak, IEEE Trans. Plasma Sci. **23**, 503 (1995).
[29] U. Kortshagen, C. Busch, and L. D. Tsendin, Plasma Sources Sci. Technol. **5**, 1 (1996).
[30] R. Winkler, F. Sigeneger, and D. Uhrlandt, Pure Appl. Chem. **68**, 1065 (1996).
[31] R. Arslanbekov, A. Kudryavtsev, and L. Tsendin, Phys. Rev. E **64**, 016401 (2001).
[32] G. A. Hebner, J. Appl. Phys. **80**, 2624 (1996).
[33] R. D. White, R. E. Robson, B. Schmidt, and M. A. Morrison, J. Phys. D **36**, 3125 (2003).
[34] I. B. Bernstein and T. Holstein, Phys. Rev. **94**, 1475 (1954).
[35] L. L. Alves, G. Gousset, and C. M. Ferreira, Phys. Rev. E **55**, 890 (1997).
[36] U. Kortshagen, Plasma Sources Sci. Technol. **4**, 172 (1995).
[37] I. P. Shkarofsky, T. W. Johnston, and M. P. Bachynski, *The Particle Kinetics of Plasmas* (Addison-Wesley, Reading, MA, 1966).
[38] R. Winkler, H. Deutsch, J. Wilhelm, and C. Wilke, Beitr. Plasmaphys. **24**, 203 (1984); **24**, 285 (1984).
[39] V. Zeman, K. Bartschat, C. Norén, and J. W. McConkey, Phys. Rev. A **58**, 1275 (1998).
[40] K. Bartschat and V. Zeman, Phys. Rev. A **59**, R2552 (1999).
[41] J. B. Boffard, G. A. Piech, M. F. Gehrke, L. W. Anderson, and C. C. Lin, Phys. Rev. A **59**, 2749 (1999).
[42] M. Schaper and H. Schreibner, Contrib. Plasma Phys. **9**, 43 (1969).
[43] D. Rapp and P. Englander-Golden, J. Chem. Phys. **43**, 1464 (1965).
[44] H. Deutsch, K. Becker, S. Matt, and T. Märk, J. Phys. B **32**, 4249 (1999).
[45] C. Yamabe, S. J. Buckman, and A. V. Phelps, Phys. Rev. A **27**, 1345 (1983).
[46] N. B. Kolokolov, A. Kudrjavtsev, and A. B. Blagoev, Phys. Scr. **50**, 371 (1994).
[47] V. A. Shevelev, V. P. Stepaniuk, and G. G. Lister, J. Appl. Phys. **92**, 3454 (2002).
[48] J. E. Lawler and U. Kortshagen, J. Phys. D **32**, 3188 (1999).
[49] U. Kortshagen and B. Heil, Appl. Phys. Lett. **77**, 1265 (2000).
[50] M. Schmidt, D. Uhrlandt, and R. Winkler, J. Comput. Phys. **168**, 26 (2001).
[51] D. Uhrlandt and St. Franke, J. Phys. D **35**, 680 (2002).
[52] S. Gortchakov, H. Lange, and D. Uhrlandt, J. Appl. Phys. **93**, 9508 (2003).
[53] J. H. Ingold, in *Gaseous Electronics*, edited by M. N. Hirsh and H. J. Oskam (Academic Press, New York, 1978).
[54] D. Uhrlandt, M. Schmidt, and R. Winkler, Comput. Phys. Commun. **118**, 185 (1999).
[55] K. G. Greenberg and G. A. Hebner, J. Appl. Phys. **73**, 8126 (1993).
[56] G. A. Hebner and P. A. Miller, J. Appl. Phys. **87**, 8304 (2000).